Discharge efficiency in high-Xe-content plasma display panels

Discharge efficiency in high-Xe-content plasma display panels

Daiyu Hayashi[a] and Gero Heusler
Philips Forschungslaboratorien Aachen, Weisshausstrasse 2, 52066, Aachen, Germany

Gerjan Hagelaar and Gerrit Kroesen
Technische Universiteit Eindhoven, P.O. Box 513, 5600 MB Eindhoven, The Netherlands

(Received 2 September 2003; accepted 26 November 2003)

We study theoretically the overall output performance and the dominating reaction processes of the vacuum ultraviolet (UV) radiation production in high-Xe partial pressures in plasma display panels (PDPs) with Ne–Xe gas mixtures. A two-dimensional self-consistent fluid model is applied for the simulations of discharges and UV radiation in sustaining phases of PDPs. The UV intensity increases with the Xe partial pressure (P_{Xe}). The discharge efficiency also increases with P_{Xe}. The resonant radiation from $\mathrm{Xe}(^3P_1)$ dominates for 3.5%, while that from $\mathrm{Xe}_2(^3\Sigma_u^+)$ becomes dominant over $\mathrm{Xe}(^3P_1)$ for 10%–30%. Remarkably for 30%, the intensity from $\mathrm{Xe}_2(^1\Sigma_u^+)$ is even larger than that from $\mathrm{Xe}(^3P_1)$. It is found that for higher P_{Xe}, the UV radiation mainly consists of the excimer radiation from $\mathrm{Xe}_2(^1\Sigma_u^+)$ and $\mathrm{Xe}_2(^3\Sigma_u^+)$. Here, $\mathrm{Xe}(^3P_1)$ does not play a role itself as the UV radiator of the resonant radiation (147 nm), but as the precursor to $\mathrm{Xe}_2(^1\Sigma_u^+)$, which results in the excimer radiation (173 nm). © *2004 American Institute of Physics.* [DOI: 10.1063/1.1641961]

I. INTRODUCTION

The plasma display panel (PDP) is regarded as the most promising candidate for the next generation of consumer-oriented, large-size, flat displays.[1,2] The major trend of the discharge scheme in PDPs is alternating current (ac), capacitive discharges between coplanar electrodes covered by dielectric materials in Xe-noble gas (He, Ar, and Ne) mixtures. Vacuum ultraviolet (UV) radiation from Xe and its excimers from the discharge is converted to visible light by phosphors, in order to display color images. In spite of elaborate efforts in research and development, considerably lower luminous efficiency, approximately by four times than that of cathode-ray-tube displays, is currently a bottleneck of PDP technology in competing against other display technologies in consumer markets. Drastic improvement of the luminous efficiency is the major and urgent objective in PDP technology.

The luminous efficiency of PDPs is given by the following four factors: (1) The discharge efficiency (hereafter, we will refer to it as η_{dis}), i.e., the yield of applied electric energy into UV photon energy via discharges ($<5\%$), (2) the probability of the UV photons to be captured by phosphor ($\sim 40\%$), (3) the quantum efficiency of phosphors ($\sim 25\%$), and (4) the yield of the visible photons reaching the display area ($\sim 40\%$), where the percentages in brackets indicate the estimated efficiencies of each factor.[3–5] Factors 2 and 4 mostly depend on the geometry of PDP cells. A relatively large Stokes shift (from ~ 143–173 nm to visible wavelength range ~ 400–700 nm) of the photon conversion scheme using UV radiation limits the quantum efficiency of factor 3 to as low as 25%. Nonetheless, the values are comparable to that in other gas-discharge light sources using similar schemes of visible photon generation. Regarding factors 2 and 4, a drastic improvement in luminous efficiency has been achieved by increasing the effective luminous areas in PDP cells.[6,7] The discharge efficiency η_{dis} is, on the other hand, extremely small compared with those of other discharges ($\sim 65\%$ in a Hg–rare-gas lamp,[8] and $\sim 60\%$ in a Xe–DBD lamp),[9] and is mainly responsible for the low luminous efficiency of PDPs. It has been clarified that the significant dissipation of the input power to ions and subsequently to neutrals is the major cause for the low η_{dis} in conventional PDPs with Xe–Ne and Xe–He gas mixtures.[4,5] This is unfortunately an intrinsic feature of cathode-fall dominated discharges, in general, which are the typical discharges generated in conventional PDP cells.[8,10] A sufficiently large ion flux to a cathode for emitting secondary electrons is inevitable to sustain the discharges. Recently, it was reported that PDPs with high-Xe-content gas mixtures have the potential for improving luminous efficiency under a conventionally used driving scheme.[11,12] The luminous efficiency exhibits a step-wise increase by increasing the sustain voltages especially for higher-Xe contents. The luminous efficiency increases linearly to total pressure. Almost all of the UV radiation consists of Xe_2 excimer emission, not of Xe resonance radiation.

In this article, we study theoretically a Xe–Ne ac-PDP for various Xe contents and describe the decisive physical process of the discharge efficiency improvement in high-Xe-content PDPs. We apply a two-dimensional, self-consistent fluid model[4] to analyze the discharge efficiency η_{dis} in a PDP cell. A focus is on the analysis of the reaction chemistry related to the UV generation. The physical description of gas discharges, and numerical techniques implemented in the two-dimensional fluid model, has been described in detail elsewhere.[4,13] We apply a boundary condition that correctly takes into account of the contribution from the secondary electron flux.[14] The reaction processes considered in the simulation are listed in Refs. 4 and 13. The imprisonment

[a]Electronic mail: daiyu.hayashi@philips.com

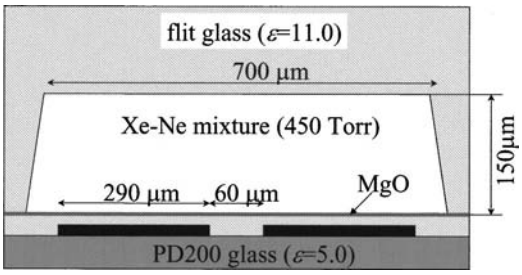

FIG. 1. A schematic geometry of the PDP cell.

effect of the Xe resonant line (147 nm) is taken into account in the simulation by introducing the escape factor[15] for the resonant radiation, which is preliminarily determined by the photon Monte Carlo simulation.[16] A standard cell structure widely used for ac-color PDPs is considered here. Simulations are performed in a two-dimensional area of the intersection of the sustain electrodes. A schematic geometry of the cell is depicted in Fig. 1. It consists of two glass plates, separated by a gap of 150 μm, filled with a Ne–Xe gas mixture. A pair of electrodes to sustain discharges (hereafter, sustaining electrodes) is placed on the front panel (at the bottom in Fig. 1). The sustaining electrodes are covered by a dielectric layer consisting of a glass plate (dielectric constant ~11.0) and MgO layer at the top (dielectric constant ~11.0). The total pressure of the gas fillings is kept constant at 450 Torr. The partial concentration of Xe (P_{Xe}) is varied from 3.5%–30%. We first apply a high voltage of 400–500 V between the sustaining electrodes to generate a preliminary discharge. Surface charges that initiate following discharges between the sustaining electrodes are built up on the dielectric layers. Then, discharges are sustained by applying a 50 kHz square ac voltage (V_s) to the sustaining electrodes. We will refer to these discharge periods as sustaining phases. The rise and decay times of V_s are typically set at 50 ns. Hereafter, we will restrict our discussions to the phenomena in the sustaining phases. The simulations are done all over on the two-dimensional cross section of Fig. 1. Toward the aim of investigating the output performance of the PDP cell, all the results presented here are integrated and averaged in a half cycle and over the cross section, unless it is otherwise mentioned.

II. OVERALL PERFORMANCE

Figure 2 shows the electric input energy (W_{in}) per half cycle of the sustaining phase as a function of V_s for $P_{\mathrm{Xe}}=3.5\%-30\%$. The W_{in} is linear to V_s and independent from P_{Xe}. Our preliminary simulation has also found a well-known relation that W_{in} is approximately proportional to the capacitance (C_{sus}) of the sustaining electrode. For the discharge conditions in this article, W_{in} is then given as a simple relation: $W_{\mathrm{in}}=A\cdot C_{\mathrm{sus}}\cdot(V_s\text{-}V_{\mathrm{min}})$, where A and V_{min} are a constant value and a certain minimum voltage (~140–170 V), respectively. It is noted that a variation with regard to V_s therefore corresponds linearly to that with regard to W_{in}.

Figure 3 schematically depicts the atomic and molecular electronic states involved in the UV radiation. Except negligibly weak emission from Ne, the UV radiation from PDPs

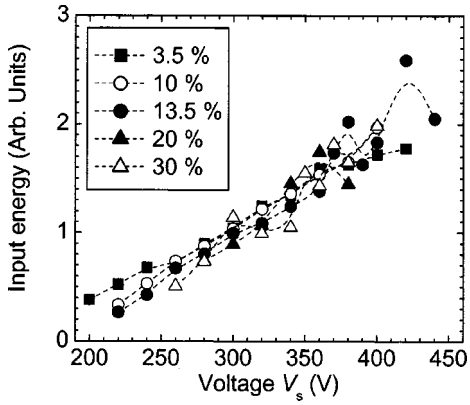

FIG. 2. The electric input energy (W_{in}) per a half cycle of the sustaining phase as a function of V_s for $P_{\mathrm{Xe}}=3.5\%-30\%$.

with a Ne–Xe mixture consists of an atomic resonant radiation, $\mathrm{Xe}(^3P_1)\rightarrow\mathrm{Xe}(^1S_0)$, and molecular radiation from three excimers, $\mathrm{Xe}_2(^3\Sigma_u^+, {}^1\Sigma_u^+, O_u^+)\rightarrow\mathrm{Xe}_2(^1\Sigma_g^+)\approx\mathrm{Xe}(^1S_0)+\mathrm{Xe}(^1S_0)$.

The total UV radiation intensities from $\mathrm{Xe}(^3P_1)$ and $\mathrm{Xe}_2(^3\Sigma_u^+, {}^1\Sigma_u^+, O_u^+)$ are shown in Fig. 4. Here, R_{UV} is the rate of the radiative transition processes generating the UV radiation, which corresponds to the number of UV photons generated per unit time. It is therefore equivalent to the photon flux intensity from the PDP. The R_{UV} increases with P_{Xe}. Whereas R_{UV} increases roughly linearly to V_s for 3.5%, R_{UV} saturates approximately at $V_s\sim350$ V for 10%–30%. This characteristic of the saturation is more remarkable for higher P_{Xe}. Choi *et al.*[15] experimentally observed the same trend in the UV intensity of the resonant line (147 nm) emissions, while the excimer emission intensity increased linearly by P_{Xe}.

We define η_{dis} as the ratio of the total UV radiation energy (W_{UV}) per half cycle to W_{in} ($\eta_{\mathrm{dis}}=W_{\mathrm{UV}}/W_{\mathrm{in}}$). The dependence of the discharge efficiency η_{dis} on V_s is shown in Fig. 5. The η_{dis} increases with P_{Xe}, as is consistent with the experimental results.[17,18] The η_{dis} exhibits a slight increase with V_s for 10% and 13.5%, and it peaks at V_s ~340 V for 20% and 30%, while no significant change is seen for 3.5%.

The η_{dis} is parametrically given by the product of the electron heating efficiency (η_e) and UV efficiency (η_{UV}).[3,4] The former represents the percentage of W_{in} to be transferred to the energy of the electrons (W_e), and the latter represents

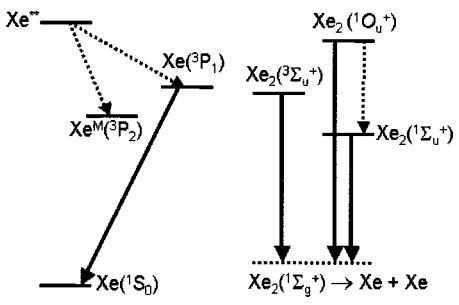

FIG. 3. The schematic diagram for the atomic and molecular electronic states involved in the UV radiation.

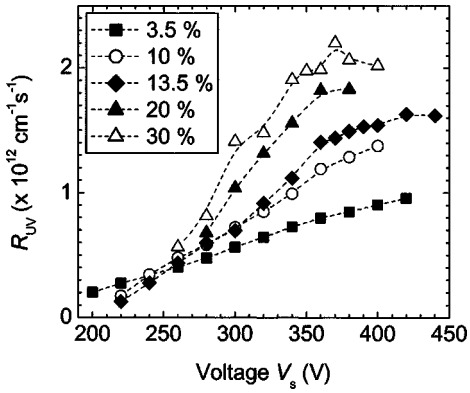

FIG. 4. The total UV radiation intensities from $Xe(^3P_1)$ and $Xe_2(^3\Sigma_u^+, {}^1\Sigma_u^+, O_u^+)$. The R_{UV} is the rate of the radiative transition processes generating the UV radiation, which corresponds to the number of UV photons generated per a unit time. It is equivalent the photon flux intensity from the PDP.

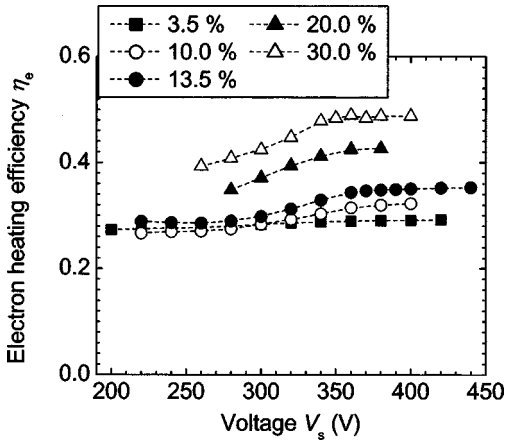

FIG. 6. The dependence of the electron heating efficiency η_e on V_s.

the percentage of W_e to be converted to the total UV radiation energy W_{UV}. Figure 6 shows the dependence of η_e on V_s. The η_e shows a step-wise increase for 10%–30%, instead of the constant value for 3.5%. The η_e is as small as approximately 27% for $P_{Xe}=3.5\%$. This means that the ion heating loss, not the electron heating, of which the efficiency is equivalent to $1-\eta_e$, predominates here. The η_e increases with P_{Xe}, 40%–50% of W_{in} is converted to the electron energy for $P_{Xe}=30\%$. Increasing P_{Xe} results in the enhancement in η_e by 1.5–1.9. It is noted that high η_e is attained for higher P_{Xe} and V_s. The UV efficiency η_{UV} is shown in Fig. 7. In the same manner as η_e, the η_{UV} increases with P_{Xe}. η_{UV} for 3.5% does not show any dependence on V_{sus}, while η_{UV} for 10%–30% shows a peak around 300 V. Thus, improvement is achieved both in η_e and η_{UV} by increasing P_{Xe}.

For all P_{Xe}, the ratios of the UV intensities from $Xe(^3P_1)$ and $Xe_2(^3\Sigma_u^+, {}^1\Sigma_u^+, O_u^+)$ relative to the total UV photon intensity show a minute change within 10% in accordance with V_s. Figure 8 shows the relative ratio of the intensity from $Xe(^3P_1)$ and $Xe_2(^3\Sigma_u^+, {}^1\Sigma_u^+, O_u^+)$ as a function of P_{Xe}. Here, we take values averaged over V_s for each P_{Xe}. The resonant radiation from $Xe(^3P_1)$ dominates for 3.5%, while that from $Xe_2(^3\Sigma_u^+)$ becomes dominant over $Xe(^3P_1)$ for 10%–30%. Remarkably for 30%, the intensity from $Xe_2(^1\Sigma_u^+)$ is even larger than that from $Xe(^3P_1)$. The ratio from $Xe(^3P_1)$ decreases with P_{Xe}. The ratios from two excimers $Xe_2(^3\Sigma_u^+, O_u^+)$ increase with P_{Xe} and saturate at 20% and 30%, while the ratio from $Xe_2(^1\Sigma_u^+)$ increases linear by P_{Xe}. When we take simply the sum of the ratios of $Xe(^3P_1)$ and $Xe_2(^1\Sigma_u^+)$, the sum is a constant value of approximately 50% and notably independent from P_{Xe}, except for the value of 3.5%.

III. REACTION SCHEME

In Sec. III., we observed the increase of η_{dis} with P_{Xe}. The parametric studies clarify that both η_e and η_{UV} increase with P_{Xe}, and η_e shows a step-wise increase with V_s while η_{UV} has a peak around $V_s=300$ V. Next, we will get insight into the reactions contributing to these behaviors of η_e and η_{UV}. Here, we restrict our discussion on the reactions for $P_{Xe}=3.5\%$ and 30%, in which two extreme conditions can be seen.

A. $P_{Xe}=3.5\%$

As can be seen in Fig. 8, the radiation from $Xe(^3P_1)$ and $Xe_2(^3\Sigma_u^+)$ dominates for 3.5%. Figure 9 shows the reaction rates of the dominating production ($r1$-$r3$) and loss ($r4$-$r7$)

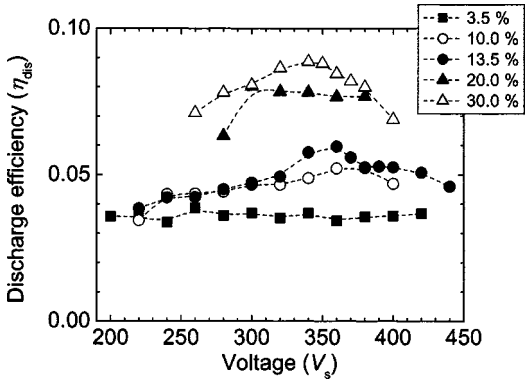

FIG. 5. The dependence of the discharge efficiency η_{dis} on V_s. We define η_{dis} as the ratio of the total UV radiation energy (W_{UV}) per a half cycle to W_{in} ($\eta_{dis}=W_{UV}/W_{in}$).

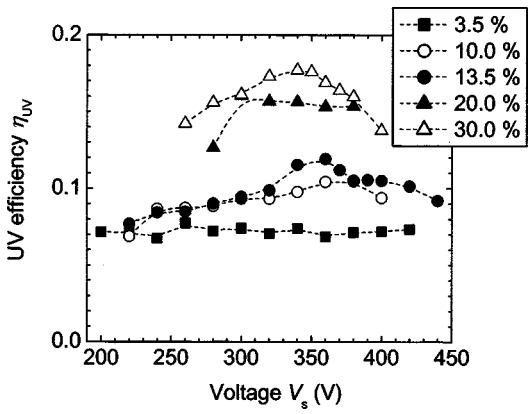

FIG. 7. The dependence of the UV efficiency η_{UV} on V_s.

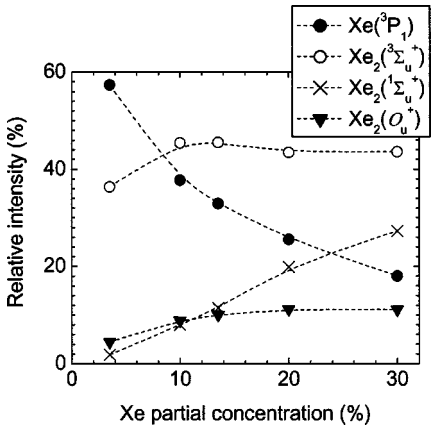

FIG. 8. The relative ratio of the intensity from $Xe(^3P_1)$ and $Xe_2(^3\Sigma_u^+, {}^1\Sigma_u^+, O_u^+)$ as a function of P_{Xe}. We take here averaged values over V_s for each P_{Xe}. The radiation from $Xe(^3P_1)$ dominates for 3.5%, while that from $Xe_2(^3\Sigma_u^+)$ becomes dominant over $Xe(^3P_1)$ for 10%–30%.

processes of $Xe(^3P_1)$ (for $V_s=240$ V). Hereafter, all of the data presented are averaged spatially over the cross section and a half-discharge-cycle period. Most of $Xe(^3P_1)$ are produced from Xe** via collision with Xe. The electron impact excitation directly from Xe contributes less. The electron impact de-excitation of $Xe(^3P_1)$ dominates in the loss reactions. Approximately one-third of the produced $Xe(^3P_1)$ is converted into the UV radiation. The molecular state $Xe_2(O_u^+)$ is produced by the three-body recombination with Xe and $Xe(^3P_1)$, $(r7)$, and converted via collisions with Ne or Xe into $Xe_2(^1\Sigma_u^+)$, of which the state mainly decays via the UV radiation. Nevertheless, the process is minority in the loss processes.

It is well known that $Xe_2(^3\Sigma_u^+)$ are produced by the three-body recombination with Xe and the metastable state $Xe(^3P_2)$, $[Xe+Xe(^3P_2)+Ne/Xe \rightarrow Xe_2(^3\Sigma_u^+)+Ne/Xe]$.[13,19,20] Our simulation also has shown that $Xe_2(^3\Sigma_u^+)$ is predominantly produced by the three-body recombination with $Xe(^3P_2)$ and lost by emitting VUV radiation. Hence, in order to study the production processes of the radiating excimer state $Xe_2(^3\Sigma_u^+)$, we study the production and loss processes of its precursor, $Xe(^3P_2)$.

Figure 10 shows the reaction rates of the production $(m1\text{-}m5)$ and loss $(m6\text{-}m9)$ processes of $Xe(^3P_2)$. Although the de-excitation of Xe** via collision with Xe $(m4,m5)$ dominates approximately half of the total production rate, the electron impact excitation $(m1)$ and de-excitation $(m2)$ processes and radiative process $(m3)$ also contribute. The main loss process is the electron impact excitation to Xe**. The three-body processes resulting in the formation of $Xe_2(^3\Sigma_u^+)$ via collisions with Ne and Xe $(m8, m9)$ are minorities and inefficient in producing $Xe_2(^3\Sigma_u^+)$ in this condition. Despite of the $Xe(^3P_2)$ production by the de-excitation of Xe** via electron impact and collisions with Ne and Xe, they are not efficiently converted to the radiative state $Xe_2(^3\Sigma_u^+)$ generating UV radiation, but mostly they are excited back to Xe** via electron impact excitation. This backward process limits the η_{dis}. The resonant radiation from $Xe(^3P_1)$, therefore, dominates, as shown in Fig. 8.

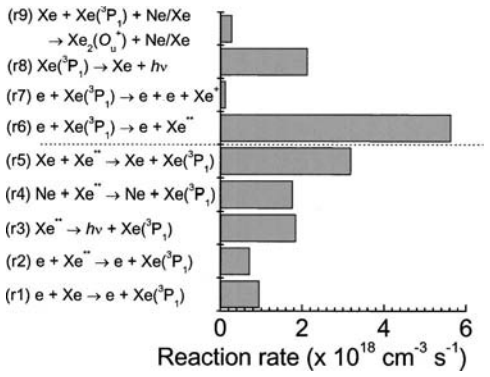

FIG. 9. The reaction rates of the dominating production $[(r1)\text{-}(r5)]$ and loss $[(r6)\text{-}(r9)]$ processes of $Xe(^3P_1)$ for $P_{Xe}=3.5\%$.

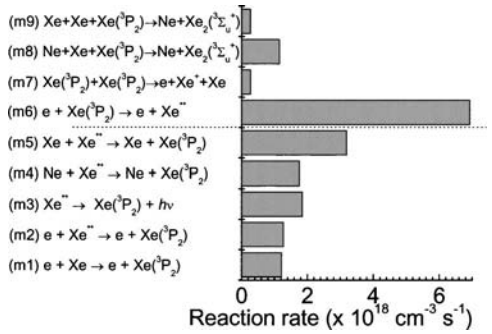

FIG. 10. The reaction rates of the production $[(m1)\text{-}(m5)]$ and loss $[(m6)\text{-}(m9)]$ processes of $Xe(^3P_2)$ for $P_{Xe}=3.5\%$.

Figure 11 schematically summarizes the reactions related to the UV generation for 3.5%. The solid lines in Fig. 11 represent the electron impact processes and the broken lines represent the reaction with the neutral species, Ne and Xe. The UV radiation mainly consists of the spontaneous emissions from $Xe(^3P_1)$ and $Xe_2(^3\Sigma_u^+)$. The direct excitations to both $Xe(^3P_1)$ and $Xe(^3P_2)$ are not dominating production processes. Due to the relatively larger cross section in comparison with those for the direct excitation of $Xe(^3P_1)$ and $Xe(^3P_2)$,[21,22] the energetic electrons collide with Xe to excite them mainly to Xe**. The main loss processes of Xe** are the collisional de-excitation to $Xe(^3P_1)$ and $Xe(^3P_2)$ with Ne and Xe (reaction rate $\sim 1\times10^{19}$ cm^3 s^{-1}), the de-excitation to $Xe(^3P_1)$ and $Xe(^3P_2)$ via spontaneous emission ($\sim 1\times10^{19}$ cm^3 s^{-1}) and the ionization processes ($\sim 1\times10^{19}$ cm^3 s^{-1}). Xe** is then converted to $Xe(^3P_1)$ and

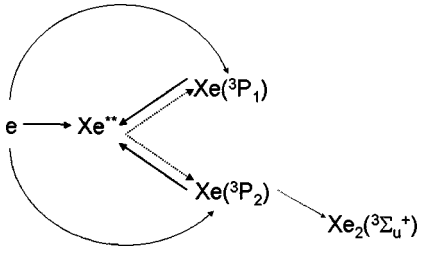

FIG. 11. The reactions related to the UV generation for 3.5%. The solid lines represent the electron impact processes and broken lines represent the reaction with the neutral species like Ne and Xe.

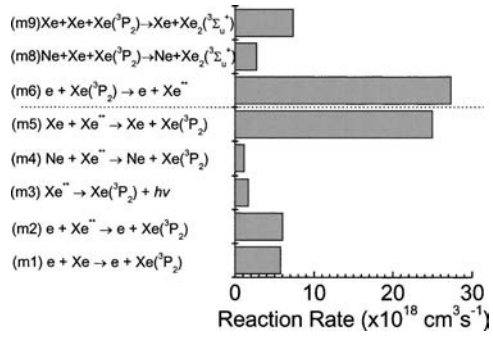

FIG. 12. The reaction rates of the production $[(m1)$-$(m5)]$ and loss $[(m6),(m8),(m9)]$ processes of $Xe(^3P_2)$ for $P_{Xe}=30\%$.

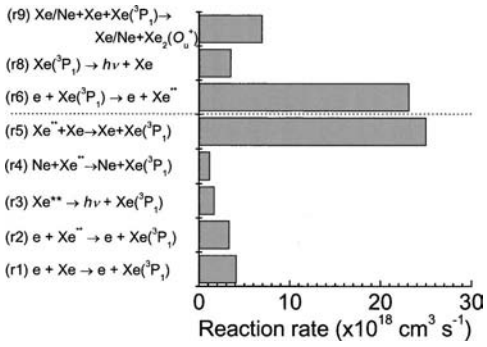

FIG. 13. The reaction rates of the production $[(r1)$-$(r5)]$ and loss processes $[(r6)$, $(r8)$, and $(r9)]$ of $Xe(^3P_1)$ for $P_{Xe}=30\%$.

$Xe(^3P_2)$ by the collosional de-excitation. Most of $Xe(^3P_1)$ are still destroyed by the electron impact excitation back to Xe**, as for $P_{Xe}=3.5\%$. Xe** is dominantly converted into $Xe(^3P_1)$ and $Xe(^3P_2)$ via collisions with Ne and Xe, in spite of the fact that electron impact de-excitation also contributes. Unfortunately, these states, being direct (resonant radiation) and indirect (excimer radiation) precursors of the UV radiation, are mostly excited back to Xe** by the electron impact excitations. The spontaneous UV emission from $Xe(^3P_1)$ and the conversion processes of $Xe(^3P_2)$ to $Xe_2(^1\Sigma_u^+)$, which finally results in the UV excimer radiation, are minor reactions.

B. $P_{Xe}=30\%$

The spontaneous emission from $Xe(^3P_1)$ is no longer dominant in the UV radiation processes. The emission processes from the two molecular states $Xe_2(^3\Sigma_u^+)$ and $Xe_2(^1\Sigma_u^+)$ are the major UV radiation processes here. As for $P_{Xe}=3.5\%$, we have confirmed that, also for $P_{Xe}=30\%$, most of $Xe_2(^3\Sigma_u^+)$ is produced by the three-body recombination of $Xe(^3P_2)$ with Xe via collisions with the third-body buffer gases (Ne and Xe). Thus, here, we study the production and loss processes of the precursor, $Xe(^3P_2)$, for $Xe_2(^3\Sigma_u^+)$. The reaction rates of the production and loss processes of $Xe(^3P_2)$ are shown in Fig. 12. The collisional de-excitation of Xe** with Xe dominates in the production process. Although the electron impact excitation back to Xe** is still the major loss process, but the conversion processes to $Xe_2(^3\Sigma_u^+)$ via collision with Ne and Xe [the reactions $(m8)$ and $(m9)$] also contribute more in comparison with those for 3.5%. The produced $Xe(^3P_2)$ is mainly converted to $Xe_2(^3\Sigma_u^+)$ that eventually generates the excimer radiation.

As is seen in Fig. 9, for $P_{Xe}=30\%$, the resonant radiation directly from $Xe(^3P_1)$ has a smaller contribution, but the excimer radiation from $Xe_2(^1\Sigma_u^+)$ rather dominates in the radiation processes involving $Xe(^3P_1)$. Here, $Xe(^3P_1)$ does not play a role as a UV radiator, but as the precursor to $Xe_2(^1\Sigma_u^+)$ becomes more dominant. Figure 13 shows the reaction rates of the production and loss processes of $Xe(^3P_1)$. Unlike for $P_{Xe}=3.5\%$, most of $Xe(^3P_1)$ is produced via collisional de-excitation of Xe** and the electron impact and radiative processes have relatively minute contributions. The electron impact de-excitation is the major loss process. The conversion process of $Xe(^3P_1)$ to $Xe_2(O_u^+)$ via the three-body collisions with Ne and Xe exhibits a larger contribution in the loss process than the radiative decay process $(r3)$. The reaction rate coefficient of the process involving Xe as the third collider is larger than that involving Ne. Hence, in the case when the Xe partial pressure is larger, the reaction rate of the reaction $(r9)$ becomes larger.

Figure 14 schematically summarizes the reactions related to the UV generation for 30%. The solid lines in Fig. 14 represent the electron impact processes and the broken lines represent the reaction with the buffer gas species, Ne and Xe. The UV radiation mainly consists of the excimer radiation from $Xe_2(^1\Sigma_u^+)$ and $Xe_2(^3\Sigma_u^+)$. Exactly in the same way as for $P_{Xe}=3.5\%$, the energetic electrons excite Xe to Xe**. The direct excitations to $Xe(^3P_1)$ and $Xe(^3P_2)$ are not the dominant production processes. The main loss processes of Xe** are the collisional de-excitation to $Xe(^3P_1)$ and $Xe(^3P_2)$ with Ne and Xe (reaction rate, $\sim 5.5\times10^{19}$ cm^3 s^{-1}), the electron impact de-excitation to $Xe(^3P_1)$ and $Xe(^3P_2)$ ($\sim 6\times10^{18}$ cm^3 s^{-1}), and the ionization processes ($\sim 2.9\times10^{19}$ cm^3 s^{-1}). The majority of Xe** is then converted to $Xe(^3P_1)$ and $Xe(^3P_2)$ by the collisional de-excitation. Most of $Xe(^3P_1)$ are still destroyed by the electron impact excitation back to Xe**, as for $P_{Xe}=3.5\%$. But some part is converted to the molecular state $Xe_2(^1O_u^+)$ via three-body collisions. $Xe_2(^1O_u^+)$ is de-excited to $Xe_2(^1\Sigma_u^+)$ via collisions with Ne and Xe, and then $Xe_2(^1\Sigma_u^+)$ eventually radiates the UV excimer emissions. $Xe(^3P_2)$ is generated from Xe** by the collisional de-excitation with Ne and Xe, and also by the electron impact de-excitation. The backward process from $Xe(^3P_2)$ to Xe** does not dominate here, but $Xe(^3P_2)$ is converted to $Xe_2(^3\Sigma_u^+)$ via three-body collisions with Xe and the buffer gases (Ne and Xe). Thus, the UV radiation in this condition is dominated by the molecular excimer radiation. It is noted

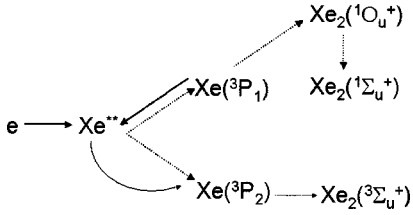

FIG. 14. The reactions related to the UV generation for 30%.

that, for $P_{Xe}=30\%$, due to the high reaction rate of mainly three-body collisions involving Xe, the forward processes toward the radiative states dominates against the backward processes, like the electron impact excitation to Xe**. Therefore, η_{UV}, the UV conversion efficiency, is higher than that for low P_{Xe}.

IV. SUMMARY

We studied the reaction processes related to the UV production in a standard Xe–Ne ac-PDP for various Xe content. The two-dimensional, self-consistent, fluid model under the proposed boundary condition is employed to investigate the discharge mechanisms in PDPs with Xe–Ne gas mixtures.

First, the overall output performance of the PDP cell is studied. The UV intensity, equivalent to R_{UV}, increases with P_{Xe}. The R_{UV} saturates approximately at $V_s \sim 350$ V for 10%–30% and the saturation character is more remarkable for higher P_{Xe}. The discharge efficiency, η_{dis}, increases with P_{Xe}. The η_{dis} peaks at $V_s \sim 340$ V for higher P_{Xe} ($=20\%$ and 30%), while no significant change is seen for $P_{Xe}=3.5\%$. The electron heating efficiency, η_e, and the UV conversion efficiency, η_{UV}, are both enhanced by increasing P_{Xe}.

The relative ratio of the UV intensities from $Xe(^3P_1)$, and $Xe_2(^3\Sigma_u^+, {}^1\Sigma_u^+, O_u^+)$ is calculated as a function of P_{Xe}. The resonant radiation from $Xe(^3P_1)$ dominates for 3.5%, while that from $Xe_2(^3\Sigma_u^+)$ becomes dominant over $Xe(^3P_1)$ for 10%–30%. Remarkably for 30%, the intensity from $Xe_2(^1\Sigma_u^+)$ is even larger than that from $Xe(^3P_1)$. The ratio from $Xe(^3P_1)$ decreases with P_{Xe}. The sum of the intensity ratios of $Xe(^3P_1)$ and $Xe_2(^1\Sigma_u^+)$ is a constant value of approximately 50% and notably independent of P_{Xe}, except for the value of 3.5%.

For the partial Xe pressures of 3.5% and 30%, where we see the extreme contrast in the relative contribution of the resonant and excimer radiation in the total UV radiation processes, we study the reaction processes of the excited Xe states [$Xe(^3P_1)$ and $Xe(^3P_2)$] which play important roles in the UV processes.

For $P_{Xe}=3.5\%$, the UV radiation mainly consists of the spontaneous emissions from $Xe(^3P_1)$ and $Xe_2(^3\Sigma_u^+)$. The direct excitations to both $Xe(^3P_1)$ and $Xe(^3P_2)$, the precursors to $Xe_2(^3\Sigma_u^+)$ are not dominant production processes. $Xe(^3P_1)$ and $Xe(^3P_2)$ are produced dominantly by collision de-excitation of Xe** with Ne and Xe, in spite of the fact that electron impact de-excitation also contributes. Most of them are unfortunately excited back to Xe** by the electron impact excitations. The spontaneous UV emission from $Xe(^3P_1)$ and the conversion processes of $Xe(^3P_2)$ to $Xe_2(^1\Sigma_u^+)$, which results finally in the UV excimer radiation, are minor reactions.

For $P_{Xe}=30\%$, the UV radiation mainly consists of the excimer radiation from $Xe_2(^1\Sigma_u^+)$ and $Xe_2(^3\Sigma_u^+)$. Here, $Xe(^3P_1)$ does not play a role as the UV radiator itself, but as the precursor to $Xe_2(^1\Sigma_u^+)$. The direct excitations to $Xe(^3P_1)$ and $Xe(^3P_2)$ are not the dominant production processes. Then, Xe** is converted into $Xe(^3P_1)$ and $Xe(^3P_2)$ via collisions with Ne and Xe. Most of $Xe(^3P_1)$ is still destroyed by the electron impact excitation back to Xe**, as for $P_{Xe}=3.5\%$. $Xe(^3P_2)$ is generated from Xe** by the collisional de-excitation with Ne and Xe, and also by the electron impact de-excitation. The backward process from $Xe(^3P_2)$ to Xe** does not dominate here, but they are converted to $Xe_2(^3\Sigma_u^+)$ via three-body collisions with Xe and the buffer gases (Ne and Xe). Thus, the UV radiation in this condition is dominated by the molecular excimer radiation. It is remarked that, for $P_{Xe}=30\%$, due to the high reaction rate of mainly three-body collisions involving Xe, the forward processes toward the radiative states dominates against the backward processes, like the electron impact excitation to Xe**. Therefore, η_{UV}, the UV conversion efficiency, is higher than that for low P_{Xe}.

ACKNOWLEDGMENTS

The authors acknowledge G. Oversluizen, S. de Zwart, M. Gilles, and T. Dekker for discussions on the discharge efficiency. One of the authors (D. H.) likes to express his gratitude to M. Klein for his valuable contributions in developing the simulation code.

[1] J.-P. Boeuf, J. Phys. D **36**, R53 (2003); A. Sobel, IEEE Trans. Plasma Sci. **19**, 1032 (1991).
[2] L. Weber, in *Flat-Panel Displays and CRTs*, edited by L. Tannas (van Nostrand Reinhold, New York, 1985) pp. 332–407.
[3] J. Meunier, P. Belenguer, and J. P. Boeuf, J. Appl. Phys. **78**, 731 (1995).
[4] G. J. M. Hagelaar, M. H. Klein, R. J. M. M. Snijkers, and G. M. W. Kroesen, J. Appl. Phys. **89**, 2033 (2001).
[5] H. Gläser, H. Bechtel, T. Jüstel, and D. U. Wiechert, J. Soc. Inf. Disp. **8**, 189 (2000).
[6] T. Komaki, H. Taniguchi, and K. Amemiya, *Proc. of IDW'99* (1999), p. 587.
[7] O. Toyoda, T. Kosaka, F. Namiki, A. Tokai, H. Inoue, and K. Betsui, in *Proc. of IDW'99* (1999), p. 599.
[8] J. F. Waymouth, *Electric Discharge Lamps* (M. I. T. Press, Massachusetts, 1971).
[9] B. Eliasson and U. Kogelschatz, Appl. Phys. B: Photophys. Laser Chem. **46**, 299 (1988).
[10] V. I. Kolobov and L. D. Tsendin, Phys. Rev. A **46**, 7837 (1992).
[11] T. Yoshikawa, A. Miyakoshi, A. Okigawa, E. Mizobata, and K. Toki, in *Proc. of IDW'00* (2000), p. 611.
[12] G. Oversluizen, S. de Zwart, S. van Heusden, and T. Dekker, *Proc. of IDW'00* (2000), p. 631.
[13] G. J. M. Hagelaar and G. M. W. Kroesen, IEEE Trans. Plasma Sci. **27**, 1606 (1999); G. J. M. Hagelaar and G. M. W. Kroesen, J. Comput. Phys. **159**, 1 (2000); G. J. M. Hagelaar, Ph.D. thesis, (Eindhoven University of Technology, Eindhoven, 2000).
[14] G. J. M. Hagelaar, F. J. de Hoog, and G. M. W. Kroesen, Phys. Rev. E **62**, 1452 (2000).
[15] T. Holstein, Phys. Rev. **72**, 1212 (1947).
[16] G. J. M. Hagelaar and G. M. W. Kroesen, Plasma Sources Sci. Technol. **9**, 605 (2000).
[17] E. H. Choi, J. C. Ahn, M. W. Moon, Y. M. C. Choi, Y. Seo, G. Cho, H. S. Uhm, K. Tachibana, K. W. Whang, and M. Kristiansen, Appl. Phys. Lett. **81**, 3341 (2002).
[18] M. F. Gillies and G. Oversluizen, J. Appl. Phys. **91**, 6315 (2002).
[19] K. Tachibana and S. Feng, J. Appl. Phys. **88**, 4967 (2000).
[20] S. Rauf and M. J. Kushner, J. Appl. Phys. **85**, 3470 (1999).
[21] P. V. Feltsan and I. P. Zapesochny, Ukr. Fiz. Zh. **13**, 205 (1968).
[22] V. Puech and S. Mizzi, J. Phys. D **24**, 1974 (1991).